CRYSTAL GROWTH & DESIGN

pubs.acs.org/crystal | Article

Selective Area Growth by Hydride Vapor Phase Epitaxy and Optical Properties of InAs Nanowire Arrays

Gabin Grégoire, Mohammed Zeghouane, Curtis Goosney, Nebile Isik Goktas, Philipp Staudinger, Heinz Schmid, Kirsten E. Moselund, Thierry Taliercio, Eric Tournié, Agnès Trassoudaine, Evelyne Gil,* Ray R. LaPierre, and Yamina André*

Cite This: *Cryst. Growth Des.* 2021, 21, 5158−5163

Read Online

ACCESS | Metrics & More | Article Recommendations

ABSTRACT: We report on the selective area growth of InAs nanowires (NWs) by the catalyst-free vapor−solid method. Well-ordered InAs NWs were grown on GaAs(111)B and Si(111) substrates patterned with a dielectric mask using hydride vapor phase epitaxy (HVPE). Vertical and high aspect ratio InAs NWs with a hexagonal shape were grown on both GaAs and Si substrates. The impact of the growth conditions on the InAs morphology was investigated. The final shape of the InAs crystal was tuned from a NW to a nanoplatelet by controlling growth conditions such as growth temperature, vapor phase composition, and mask pattern. The influence of the aperture size on the nucleation density and then on the morphology of InAs is discussed. Small openings resulted in the formation of a single nucleus per hole, which was then converted to a NW. For larger apertures, the number of nuclei increased, leading to both three-dimensional crystals and NWs. The effect of growth temperature and the III/V ratio on the kinetics and thermodynamics of InAs growth is also discussed. The growth was first optimized on a GaAs(111)B substrate and then performed on Si, which is more suitable to develop devices. Finally, the absorbance and photoluminescence measurements were carried out on the InAs NW arrays, demonstrating the high potential of HVPE-grown InAs NWs for future multispectral photo-detection devices.

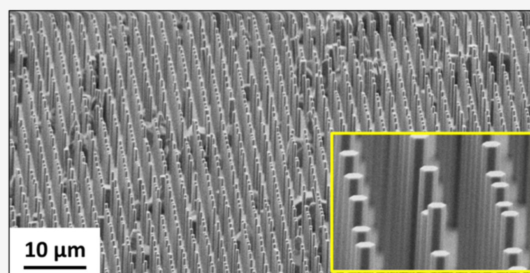

Downloaded via UNIV CLERMONT AUVERGNE on October 13, 2021 at 07:39:42 (UTC).
See https://pubs.acs.org/sharingguidelines for options on how to legitimately share published articles.

1. INTRODUCTION

The InAs semiconductor material is of great interest due to its narrow band gap, small electron effective mass, and very high electron mobility.[1] These unique properties have made the InAs material a very good candidate for ultra-high-speed electronic and optoelectronic devices. However, the monolithic integration of high-quality InAs-based materials with silicon (Si) remains a complex task in the semiconductor technology.[2] The large epitaxial strain generated by the high lattice mismatch (11.4%)[3] and the difference in thermal expansion between InAs and Si leads to surface roughness and high threading-dislocation density, which degrade the electrical and optical properties. To this end, the one-dimensional (1D) nanowire (NW) structure provides an alternative method to integrate III−V materials with Si. Owing to the small contact area with the substrate, strains are relaxed within a few atomic layers at the interface, enabling the heteroepitaxy of high-quality single-crystalline III−V NWs on the Si substrate.

Controlling the length and the diameter of NWs is essential to have homogeneous optical and electrical properties across the substrate. Selective area growth (SAG), which uses a patterned dielectric mask, is a powerful solution to control the nanostructure morphology. The SAG of InAs NWs has already been demonstrated by molecular beam epitaxy (MBE) and metal−organic vapor phase epitaxy (MOVPE) on various substrates, such as patterned InAs(111)B,[4] GaAs(111)B,[5] and Si(111).[6,7] The control of the morphology is achieved by tuning different growth parameters (growth temperature, growth time, and III/V ratio). SAG is more restricted in MBE compared to MOVPE due to the lower desorption of group-III atoms from the dielectric mask. Thus, SAG-MBE is only achieved when sufficient atom diffusivity is reached.[6] Moreover, MOVPE offers a faster growth rate due to the enhanced surface diffusion and higher material input.

Hydride vapor phase epitaxy (HVPE) is the third technique that can be used for the selective growth of micro- and nanostructures for both III-nitride and III-arsenide materials.[8−12] Due to the use of chloride III-elements, HVPE enables a perfect selectivity at a low temperature of about 600 °C on usual masks such as SiO_x or SiN_x. In refs 8 and 9, it is shown that the morphology of the microstructure can be easily tuned

Received: May 4, 2021
Revised: July 15, 2021
Published: July 27, 2021

ACS Publications © 2021 American Chemical Society

by changing the surface kinetics of the different facets. This is achievable by tight control of the growth parameters such as the temperature and III/V ratio.

We have recently reported the HVPE growth of InAs NWs on silicon substrates with high growth rates.[13] However, random nucleation due to the reoxidation of the substrate made it difficult to control the NW morphology.

In this work, we present the growth of well-ordered catalyst-free InAs NWs on GaAs and Si substrates by SAG-HVPE with very high selectivity. To the best of our knowledge, this is the first report of SAG-HVPE of InAs NWs on Si. The selectivity is ensured by patterned SiN_x and SiO_x masks deposited on Si(111) and GaAs (111)B substrates. We demonstrate the suitability of HVPE for controlling the morphology of the NWs, which is the key ingredient for multispectral infrared photo-detection.

2. EXPERIMENTAL SECTION

The SAG of InAs NWs was performed on Si(111) and GaAs(111)B substrates. This study was performed through two steps. First, the growth was calibrated on patterned GaAs(111)B substrates as condensation readily occurs on GaAs. Then, growth was performed on Si to demonstrate the feasibility of InAs-based devices on Si. The SiO_x mask was deposited on GaAs(111)B by plasma-enhanced chemical vapor deposition (PECVD), and the pattern was defined by electron beam lithography (EBL). The SiN_x mask was deposited on Si(111) by PECVD and then patterned by optical lithography. A hole diameter of 60 nm was used on GaAs(111)B. For Si(111), larger diameters were used, 350 and 500 nm, to favor nucleation. Before growth, Si(111) substrates were HF etched for 10 s to remove the native oxide formed in the openings. The substrates were then introduced in a custom HVPE reactor working at atmospheric pressure with H_2 as a carrier gas. The reactor is divided into three zones, heated by a six-zone furnace. The indium chloride (InCl) gaseous species are introduced in the source zone by flowing HCl gas on a liquid indium bath at 700 °C. Arsine (AsH_3) is introduced in the downstream central zone of the reactor heated at a higher temperature to ensure homogeneous mixing of the gas phase and reduce parasitic nucleation upstream of the substrate. AsH_3 decomposed into As_4 species when introduced into the hot-wall reactor. The substrate is placed in a downstream growth zone kept at a lower temperature than the central zone. In the following, we will discuss the results as a function of the III/V ratio, calculated as the ratio between the partial pressure of gaseous InCl and the partial pressure of gaseous As_4 in the growth zone.

The morphology of the as-grown InAs NWs was studied using a Carl Zeiss Supra scanning electron microscope with an acceleration voltage of 3 kV.

Fourier transform infrared (FTIR) spectroscopy was performed on the InAs NW arrays at room temperature using a BRUKER Hyperion 3000 system with a halogen source and mercury cadmium telluride detector. Absorptance spectra ($A(\lambda)$) were calculated as $A(\lambda) = 1 - R(\lambda) - T(\lambda)$, where the reflectance spectra $[R(\lambda)]$ and transmittance spectra $[T(\lambda)]$ were measured with a 15× objective lens. A knife-edge aperture was used to ensure the illumination of the array only. A gold-coated glass slide was used as a reference for reflectance measurements, and unobstructed air was used as a reference for transmittance measurements.

Photoluminescence (PL) spectroscopy was performed using a Brucker-Vertex 70 FTIR spectrometer equipped with a KBr beam-splitter and a cooled InSb detector. PL was excited by a 780 nm laser diode. The samples were cooled at 10K using a closed cycle He flow cryostat.

3. RESULTS AND DISCUSSION

Figure 1a,b shows tilted-view SEM images of InAs NWs grown on GaAs(111)B and Si(111) substrates, respectively. The NWs clearly exhibited a uniform diameter with a hexagonal cross section delimited by six equivalent $\{1\bar{1}0\}$ side facets and (111)B facet on the top. For both Si(111) and GaAs(111)B substrates, the NWs nucleated randomly on the edge of the openings and do not fill all the opening areas for the Si substrate. This step-edge nucleation behavior is typical for site-selective nanostructures.[14]

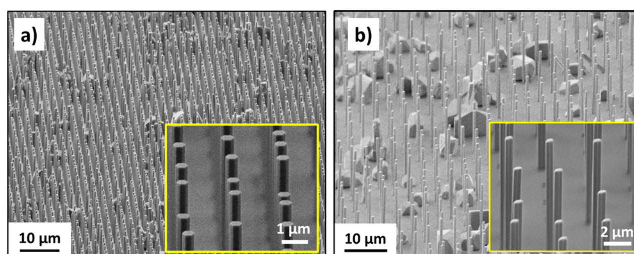

Figure 1. Tilted-view SEM images of InAs NWs grown on the (a) GaAs(111)B substrate and (b) Si(111) substrate. Hole diameters are 60 and 350 nm, respectively. Insets show a magnified view of the NWs.

Due to the non-polarity of the Si(111) surface, pre-treatment is needed to control the growth direction of the NWs. It has been demonstrated by Tomioka et al.[15] that it is possible to change the non-polar Si(111) surface to an As-terminated 1 × 1 surface by exposing the (111) surface to arsenic atoms. This procedure is now widely used by different growth techniques and seems to lead to better NW nucleation on the substrate. In HVPE, arsenic pre-treatment improves both the nucleation density and growth direction of the NWs. In this process, the direct condensation of the InAs material on Si(111) is not a straightforward process due to the low adsorption of chloride precursors in the range of temperature used in this work. The growth process is generally described by the adsorption of InCl molecules on the As-terminated surface, leading to the formation of an AsInCl molecule. This step is followed by the dechlorination of AsInCl to produce the InAs crystal.[13] The As-terminated (111)B surface of the GaAs(111)B substrate ensures the nucleation and then the growth of perfectly aligned NWs along the (111)B direction, regardless of the growth conditions. NW growth was observed on GaAs(111)B after InCl exposure, while no growth was observed on the patterned Si(111) substrate after the same pre-treatment. It highlights the importance of the arsenic surface preparation to ensure the nucleation and the growth of vertical InAs NWs on Si(111).

Figure 2 shows the SEM images of InAs micro- and nanostructures grown on the GaAs(111)B substrate with a SiO_x mask at different opening diameters (D) of (a) D = 200 nm, (b) D = 100 nm, and (c) D = 60 nm. The two-dimensional (2D) growth is observed for diameters ≥ 100 nm (Figure 2a), while NWs are obtained for the opening diameter below 100 nm (Figure 2c). Radial growth was favored for large apertures, whereas axial growth was favored for small apertures. The presence of both 2D growth and NWs in Figure 2b may be explained by residual SiO_x in the opening, resulting in a reduced hole diameter. This small effective oxide free surface is favorable for NW growth.

The nucleation density during SAG depends not only on the growth temperature and vapor-phase composition but also on the aperture size.[16,17] For large apertures, more atoms are collected enabling the nucleation of many triangular islands. The coalescence of islands during growth leads to the

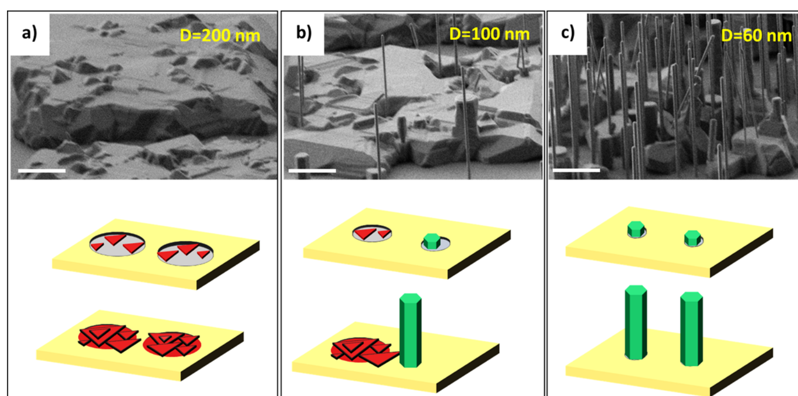

Figure 2. Tilted-view SEM images of the InAs material grown on patterned GaAs(111)B with the SiO_x mask. The corresponding schematic of the nucleation step is shown below each SEM image. The diameters of the holes were (a) 200, (b) 100, and (c) 60 nm. Different nuclei merge into coalesced triangular islands (red) or NWs (green). The pitch is 2 μm and scale bars are 5 μm.

formation of lateral facets with a very high growth rate (see the scheme in Figure 2a). Then, due to the lateral overgrowth, crystals from different apertures coalesced forming a layer with visible triangular 3D islands. In HVPE, it is well known that there is no parasitic nucleation on the dielectric mask due to the use of III-chloride precursors and the high growth temperature. For small apertures (<100 nm), only one island nucleates promoting the growth of a NW with a low radial growth rate (see the scheme in Figure 2c).

Figure 3a,b shows the SEM images of InAs NWs grown on the SiN_x-patterned Si(111) substrate with opening diameters

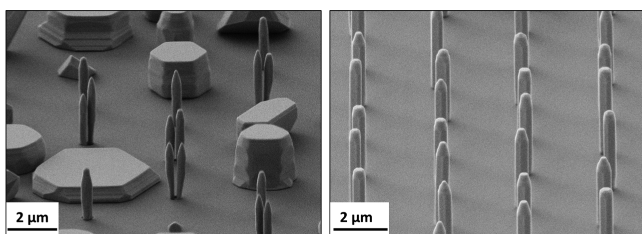

Figure 3. Tilted-view SEM images of the InAs material grown on patterned Si(111) with a SiN_x mask. The diameters of the hole are (a) 500 nm and (b) 350 nm. The pitch is 2.5 μm.

of D = 500 nm (Figure 3a) and D = 350 nm (Figure 3b). For D = 500 nm, either 3D crystals or NWs nucleated. However, for 350 nm openings, NW growth was promoted and only one NW nucleated per hole. This behavior is similar to that observed on GaAs(111)B. However, the transition between 3D growth and NW growth on Si(111) was not clearly defined and NWs grew even on very large apertures.

For growth on Si(111), we consider that for holes with 3D crystals, the same growth, as shown in Figure 2a occurs, corresponding to the coalescence of 2D islands. For holes with NWs, we speculate that the reoxidation of the surface creates pinholes inside the apertures which forms nucleation sites for NWs but inhibits the formation of large crystals. This oxidation occurs during the introduction of the sample in the reactor after the HF cleaning. Due to this reoxidation, there is a reduction of the atoms' collection area. Thus, for D = 350 nm, the oxide-free surface enables the nucleation of only one NW. Moreover, once a NW nucleates in the apertures, it acts as a sink and collects a large amount of the arriving atoms. Subsequently, the probability for additional NWs to nucleate in each hole is drastically reduced.[16]

This study highlights the lower nucleation density on Si(111) as compared to GaAs(111)B. A maximum diameter of 60 nm was required to nucleate only one NW on GaAs(111)B, while holes with a diameter of 350 nm on Si(111) still resulted in only a single NW. This is explained by the As-terminated surface of the GaAs(111)B substrate, which promotes the nucleation of the InAs material.

In HVPE, the as-grown morphology is governed by the intrinsic growth anisotropy of the crystal, that is by the growth rates of the crystal facets which depend on their surface energies. Based on simple Wulff constructions, E. Gil-Lafon et al.[8] demonstrated that HVPE growth is mainly governed by the kinetics of adsorption/desorption of the different species and the dechlorination kinetics of the ad-species. Thus, by precisely choosing the growth parameters, it is possible to easily control the morphology of the grown structures. Figure 4a shows the variation of the axial and radial growth rates of InAs NWs grown on the patterned Si(111) substrate with the growth temperature. A diameter of 350 nm was chosen to ensure the

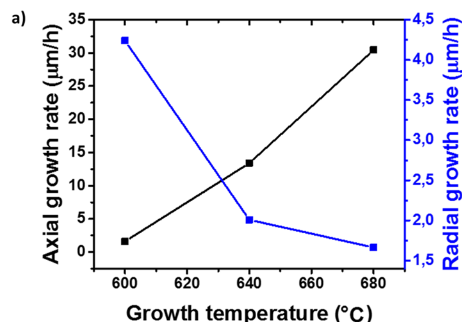

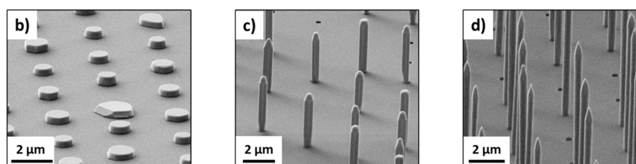

Figure 4. (a) NW length and diameter as a function of the growth temperature. Tilted-view SEM images of InAs NWs grown on the Si(111) substrate at different growth temperatures: (b) 600, (c) 640, and (d) 680 °C. The diameter of the hole is 350 nm and the pitch is 2.5 μm.

https://doi.org/10.1021/acs.cgd.1c00518
Cryst. Growth Des. 2021, 21, 5158−5163

nucleation of only one NW in the apertures. The growth temperature ranged from 600 to 680 °C and the III/V ratio was fixed at 2.

The axial growth rate increased from 1 to 32 μm/h upon increasing growth temperature from 600 to 680 °C. At low temperatures, the growth is limited by the decomposition of the adsorbed precursors, for example, dechlorination of the InCl species. As the temperature increases, the growth rate increases due to the thermal activation of the dechlorination step. This increase of the axial growth rate with increasing temperature is consistent with the kinetic model developed in ref 13 for the catalyst-free growth of InAs NWs on bare Si(111). It confirms that NWs grow following the vapor−solid mechanism.

The radial growth rate decreased with increasing temperature. In HVPE, it is assumed that the {1−10} facets have a low growth rate due to their atomic arrangement. It has been demonstrated in the case of GaAs growth that growth on {1−10} facets is mainly limited by the kinetics of adsorption and desorption of Ga and As species.[8] The same assumption can be applied to InAs growth because the growth steps are assumed to be identical with similar kinetic behavior. Thus, at low temperatures, more As and In atoms are adsorbed on the surface corresponding to a high growth rate. As we increase the temperature, the desorption increases leading to a drop of the radial growth rate. Finally, an experiment at 715 °C was also carried out where no nucleation was observed. At such growth temperatures, the desorption rate is too high to enable the nucleation of the InAs material on Si(111).

Figure 5 shows the variation of the axial and radial growth rates of NWs grown on Si(111) at 640 °C and different III/V ratios. The hole diameter was 350 nm. By increasing the III/V ratio from 2 to 6.5, we observe a slight decrease of the axial growth rate, while the radial growth rate stays nearly constant. At a higher III/V ratio, the axial growth rate decreased to 2 μm/h, and the radial growth rate increased significantly.

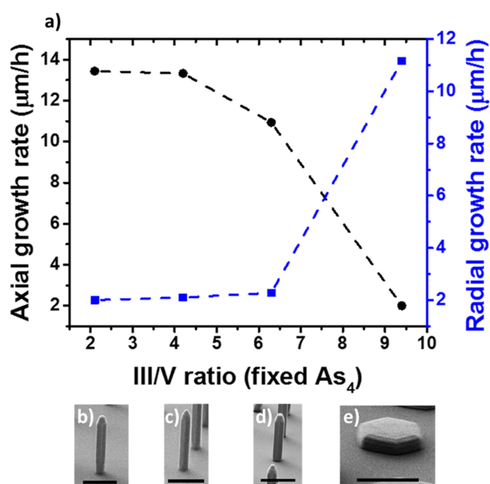

Figure 5. (a) NW radial and axial growth rates as a function of the III/V ratio. Tilted-view SEM images of InAs NW grown on Si(111) at III/V ratios: (b) 2, (c) 4.5, (d) 6.5, and (e) 9.5. Scale bars are 2 μm. The diameter of the hole is 350 nm and the pitch is 2.5 μm.

The growth of the top (111)B facet is mainly limited by the supersaturation of the vapor phase, that is, by the gaseous material input with respect to the equilibrium of the deposition reaction, and by the dechlorination of the adsorbed InCl. It is shown in ref 13 that the axial growth rate first increases by increasing the InCl partial pressure which results in higher supersaturation. When the InCl partial pressure becomes too high, the surface starts to be blocked by undecomposed AsInCl molecules and the growth rate reaches a plateau. InAs NWs were grown here at III/V ratios greater than 2, corresponding to the saturation regime that leads to a decrease of the axial growth rate once the III/V ratio is 4. For the III/V ratio between 2 and 4, the axial growth rate is at its maximum value. As we increase the InCl partial pressure, the axial growth rate starts to decrease. Further increase of the InCl partial pressure (III/V = 9.5) leads to a drastic change of the InAs crystal morphology. At high III/V ratios, the (111)B facet becomes saturated by the AsInCl molecules, which inhibits the axial growth rate. On the other hand, the radial growth rate strongly increased with the III/V ratio. An increase of the InCl adsorption on the {1−10} facets does not explain such a variation of the morphology. It is well known that the growth rate of the {1−10} facets is mainly dependent on the adsorption of As atoms. Björk et al.[7] demonstrated that the number of nuclei inside an aperture is a function of the flux of In atoms. A minimum In flux was needed to have the nucleation of a single NW in the aperture. By further increasing the In flux, they observed multiple NW nucleations. In our case, we assume that by increasing the InCl partial pressure, we enhance the nucleation density, leading to many nuclei in the hole. Thus, as explained previously, the coalescence of the different islands forms new facets with a high growth rate.

Low-temperature PL spectra of InAs NWs grown on GaAs(111)B and Si(111) are shown in Figure 6a,b, respectively. For NWs grown on GaAs(111)B, a strong peak at 0.445 eV with a full width at half-maximum (fwhm) of 32 meV was observed, designated as a_1. NWs grown on Si exhibited a dominant PL emission centered at 0.413 eV with a fwhm of 34 meV, designated as a_2. A lower PL intensity recorded from InAs NWs grown on Si compared to GaAs is probably due to the lower NW density and diameter.

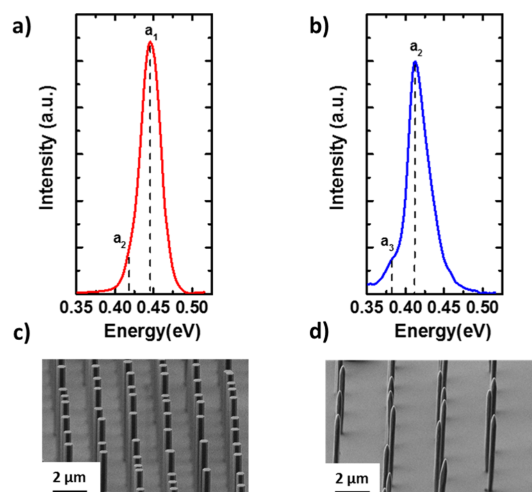

Figure 6. PL spectra at 10 K of InAs NWs grown on (a) GaAs(111)B and (b) Si(111). (c,d) Corresponding SEM images. The pitches are, respectively, 2 and 2.5 μm.

The PL peak energy a_1 (0.445 eV) shown in Figure 6a is blue-shifted compared to that of bulk zinc blende (ZB) InAs at 0.418 eV. Similar peak energies have already been observed in the literature. Koblmüller et al.[18] observed a shift of the PL

spectra when varying the NW diameter. By decreasing the NW diameter, the principal PL peak shifted to a higher energy. This blue shift is attributed to the quantum confinement (QC) of very thin InAs NWs (~50 nm). However, the NWs studied here are too large (~350 nm) to exhibit QC.

In refs 19−21, a PL peak between 0.45 and 0.48 eV was associated with wurtzite (WZ)-dominated and mixed WZ-ZB InAs NWs. This was supported by Bechstedt and Belabbes[22] who estimated the band gap energy for different polytypes (0.411, 0.431, 0.440, and 0.481 eV for the 3C, 6H, 4H, and 2H polytypes, respectively). The presence of both cubic and hexagonal phases has already been observed in InAs NW grown by HVPE.[13] The PL peak emission a_2 observed at 0.418 eV is probably due to the contribution of the ZB phase of InAs, confirming the presence of both WZ and ZB phases in InAs NWs grown by SAG-HVPE. The dominant PL peak energy a_2 at 0.413 eV of InAs NW grown on Si, as shown in Figure 6b, corresponds to the ZB band-to-band transition, and the shoulder a_3 observed at 0.38 eV is attributed to the emission from defects.[23]

To further explore the potential of InAs NWs for optical applications, especially photodetectors, we examined their optical absorptance, as measured by FTIR spectroscopy. For this purpose, NWs were grown on high resistivity (5×10^7 Ωcm) GaAs(111)B substrates to avoid free-carrier absorption from the substrate. FTIR spectra are shown in Figure 7 for three different NW diameters (310, 530, and 630 nm).

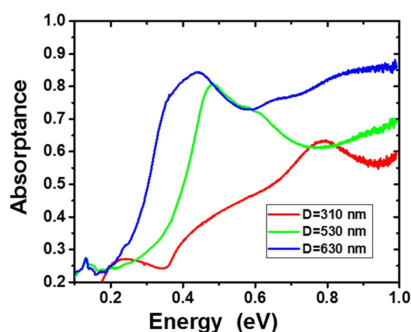

Figure 7. Room-temperature FTIR spectra of InAs NWs with different diameters (D) at constant pitch (4 μm).

The FTIR spectra exhibited strong optical absorptance with a primary absorptance peak that red-shifted with increasing NW diameter. The NW support leaky mode resonances (primarily HE_{11} modes), resulting in strong optical absorption at certain resonant wavelengths.[24,25] The absorption peak red-shifts with the increasing NW diameter due to the electromagnetic boundary conditions, indicating that these NW arrays might be useful for multispectral infrared photodetectors.[24,25] Based on prior simulations,[25] the HE_{11} resonance peak is expected at 0.81, 0.56, and 0.49 eV for InAs NWs of diameters 310, 530, and 630 nm, respectively, in a reasonable agreement with the experimental results shown in Figure 7. The resonance peaks broaden with increasing diameter, possibly due to near-field coupling between adjacent NWs.[26] In addition, FTIR results may be affected by scattering. In the absence of scattering, FTIR measurements agree almost perfectly with simulated spectra.[27] Scattering, if present, results in a loss of light and an apparent increase in absorptance. Thus, scattering from parasitic growth likely resulted in some background absorptance in the measured FTIR spectra.

CONCLUSIONS

In this work, we demonstrated the SAG of InAs NWs on GaAs(111)B and Si(111) using the HVPE technique. NWs grew vertically from GaAs(111)B or Si(111) substrates and exhibited a high aspect ratio. The morphology of the grown material depends on the growth conditions and the size of the apertures. The morphology versus growth conditions was described by considering the kinetics of the growth mechanisms involved in HVPE. The PL spectra confirmed the presence of both ZB and wurtzite structures. However, the NW arrays exhibited strong PL intensity and optical absorption, which is encouraging for future optical devices on silicon.

AUTHOR INFORMATION

Corresponding Authors

Evelyne Gil − *Université Clermont Auvergne, CNRS, Clermont Auvergne INP, Institut Pascal, Clermont-Ferrand F-63000, France*; Email: yamina.andre@uca.fr

Yamina André − *Université Clermont Auvergne, CNRS, Clermont Auvergne INP, Institut Pascal, Clermont-Ferrand F-63000, France*; Email: evelyne.gil@uca.fr

Authors

Gabin Grégoire − *Université Clermont Auvergne, CNRS, Clermont Auvergne INP, Institut Pascal, Clermont-Ferrand F-63000, France*; orcid.org/0000-0002-2183-3568

Mohammed Zeghouane − *Université Clermont Auvergne, CNRS, Clermont Auvergne INP, Institut Pascal, Clermont-Ferrand F-63000, France*; orcid.org/0000-0002-2268-5106

Curtis Goosney − *Department of Engineering Physics, McMaster University, Hamilton L8S4L7 Ontario, Canada*

Nebile Isik Goktas − *Department of Engineering Physics, McMaster University, Hamilton L8S4L7 Ontario, Canada*

Philipp Staudinger − *IBM Research Europe, 8803 Rüschlikon, Switzerland*

Heinz Schmid − *IBM Research Europe, 8803 Rüschlikon, Switzerland*; orcid.org/0000-0002-0228-4268

Kirsten E. Moselund − *IBM Research Europe, 8803 Rüschlikon, Switzerland*

Thierry Taliercio − *IES, Univ. Montpellier, CNRS, Montpellier F-34000, France*

Eric Tournié − *IES, Univ. Montpellier, CNRS, Montpellier F-34000, France*; orcid.org/0000-0002-8177-0810

Agnès Trassoudaine − *Université Clermont Auvergne, CNRS, Clermont Auvergne INP, Institut Pascal, Clermont-Ferrand F-63000, France*

Ray R. LaPierre − *Department of Engineering Physics, McMaster University, Hamilton L8S4L7 Ontario, Canada*; orcid.org/0000-0003-4598-8940

Complete contact information is available at: https://pubs.acs.org/10.1021/acs.cgd.1c00518

Author Contributions

The manuscript was written through contributions of all the authors. All the authors have given approval to the final version of the manuscript.

Notes

The authors declare no competing financial interest.

■ ACKNOWLEDGMENTS

This work was supported by Région Auvergne Rhône-Alpes; Pack ambition recherche; and Convention n°17 011236 01-61617. The authors thank 2MAtech, Aubiere, France, for scanning electron microscopy measurements. This work also received funding from the H2020 ERC POC project ENUF, grant number 790448. It was also funded by the program "Investissements d'avenir" of the French ANR agency, the French government IDEX-SITE initiative 16-μIDEX-0001 (CAP20- 25), the European Commission (Auvergne FEDER Funds), and the Region Auvergne in the framework of the LabEx IMobS3 (ANR-10-LABX-16-01). C.G., N.I.G., and RRL acknowledge the financial support of the Natural Sciences and Engineering Research Council of Canada from grants RGPIN-2018-04015 and RGPAS-2018-522624.

■ REFERENCES

(1) Gupta, N.; Song, Y.; Holloway, G. W.; Sinha, U.; Haapamaki, C. M.; LaPierre, R. R.; Baugh, J. Temperature-Dependent Electron Mobility in InAs Nanowires. *Nanotechnology* **2013**, *24*, 225202.

(2) Gorji Ghalamestani, S.; Berg, M.; Dick, K. A.; Wernersson, L.-E. High Quality InAs and GaSb Thin Layers Grown on Si (111). *J. Cryst. Growth* **2011**, *332*, 12−16.

(3) Ohtake, A.; Mano, T.; Sakuma, Y. Strain Relaxation in InAs Heteroepitaxy on Lattice-Mismatched Substrates. *Sci. Rep.* **2020**, *10*, 4606.

(4) Tomioka, K.; Mohan, P.; Noborisaka, J.; Hara, S.; Motohisa, J.; Fukui, T. Growth of Highly Uniform InAs Nanowire Arrays by Selective-Area MOVPE. *J. Cryst. Growth* **2007**, *298*, 644−647.

(5) Paetzelt, H.; Gottschalch, V.; Bauer, J.; Benndorf, G.; Wagner, G. Selective-area growth of GaAs and InAs nanowires-homo- and heteroepitaxy using templates. *J. Cryst. Growth* **2008**, *310*, 5093−5097.

(6) Hertenberger, S.; Rudolph, D.; Bichler, M.; Finley, J. J.; Abstreiter, G.; Koblmüller, G. Growth Kinetics in Position-Controlled and Catalyst-Free InAs Nanowire Arrays on Si(111) Grown by Selective Area Molecular Beam Epitaxy. *J. Appl. Phys.* **2010**, *108*, 114316.

(7) Björk, M. T.; Schmid, H.; Breslin, C. M.; Gignac, L.; Riel, H. InAs nanowire growth on oxide-masked ⟨111⟩ silicon. *J. Cryst. Growth* **2012**, *344*, 31−37.

(8) Gil-Lafon, E.; Napierala, J.; Castelluci, D.; Pimpinelli, A.; Cadoret, R.; Gérard, B. Selective Growth of GaAs by HVPE: Keys for Accurate Control of the Growth Morphologies. *J. Cryst. Growth* **2001**, *222*, 482−496.

(9) Napierala, J.; Gil-Lafon, E.; Castelluci, D.; Pimpinelli, A.; Gérard, B. Control of the Growth Morphologies of GaAs Stripes Grown on Patterned Substrates by HVPE. *Opt. Mater.* **2001**, *17*, 315−318.

(10) Tourret, J.; Gourmala, O.; André, Y.; Trassoudaine, A.; Gil, E.; Castelluci, D.; Cadoret, R. A Complete Crystallographic Study of GaN Epitaxial Morphologies in Selective Area Growth by Hydride Vapour Phase Epitaxy (SAG-HVPE). *J. Cryst. Growth* **2009**, *311*, 1460−1465.

(11) Lekhal, K.; Bae, S.-Y.; Lee, H.-J.; Mitsunari, T.; Tamura, A.; Deki, M.; Honda, Y.; Amano, H. Controlled Morphology of Regular GaN Microrod Arrays by Selective Area Growth with HVPE. *J. Cryst. Growth* **2016**, *447*, 55−61.

(12) Zeghouane, M.; Avit, G.; Cornelius, T. W.; Salomon, D.; André, Y.; Bougerol, C.; Taliercio, T.; Meguekam-Sado, A.; Ferret, P.; Castelluci, D.; Gil, E.; Tournié, E.; Thomas, O.; Trassoudaine, A. Selective Growth of Ordered Hexagonal InN Nanorods. *CrystEngComm* **2019**, *21*, 2702−2708.

(13) Grégoire, G.; Gil, E.; Zeghouane, M.; Bougerol, C.; Hijazi, H.; Castelluci, D.; Dubrovskii, V. G.; Trassoudaine, A.; Goktas, N. I.; LaPierre, R. R.; André, Y. Long Catalyst-Free InAs Nanowires Grown on Silicon by HVPE. *CrystEngComm* **2021**, *23*, 378−384.

(14) Portavoce, A.; Hull, R.; Reuter, M. C.; Ross, F. M. Nanometer-Scale Control of Single Quantum Dot Nucleation through Focused Ion-Beam Implantation. *Phys. Rev. B* **2007**, *76*, 235301.

(15) Tomioka, K.; Motohisa, J.; Hara, S.; Fukui, T. Control of InAs Nanowire Growth Directions on Si. *Nano Lett.* **2008**, *8*, 3475−3480.

(16) Mandl, B.; Dey, A. W.; Stangl, J.; Cantoro, M.; Wernersson, L.-E.; Bauer, G.; Samuelson, L.; Deppert, K.; Thelander, C. Self-Seeded, Position-Controlled InAs Nanowire Growth on Si: A Growth Parameter Study. *J. Cryst. Growth* **2011**, *334*, 51−56.

(17) Tomioka, K.; Kobayashi, Y.; Motohisa, J.; Hara, S.; Fukui, T. Selective-area growth of vertically aligned GaAs and GaAs/AlGaAs core-shell nanowires on Si(111) substrate. *Nanotechnology* **2009**, *20*, 145302.

(18) Koblmüller, G.; Vizbaras, K.; Hertenberger, S.; Bolte, S.; Rudolph, D.; Becker, J.; Döblinger, M.; Amann, M.-C.; Finley, J. J.; Abstreiter, G. Diameter Dependent Optical Emission Properties of InAs Nanowires Grown on Si. *Appl. Phys. Lett.* **2012**, *101*, 053103.

(19) Sonner, M.; Treu, J.; Saller, K.; Riedl, H.; Finley, J. J.; Koblmüller, G. Carrier Concentration Dependent Photoluminescence Properties of Si-Doped InAs Nanowires. *Appl. Phys. Lett.* **2018**, *112*, 091904.

(20) Rota, M. B.; Ameruddin, A. S.; Fonseka, H. A.; Gao, Q.; Mura, F.; Polimeni, A.; Miriametro, A.; Tan, H. H.; Jagadish, C.; Capizzi, M. Bandgap Energy of Wurtzite InAs Nanowires. *Nano Lett.* **2016**, *16*, 5197−5203.

(21) Chen, X.; Zhuang, Q.; Alradhi, H.; Jin, Z. M.; Zhu, L.; Chen, X.; Shao, J. Midinfrared Photoluminescence up to 290 K Reveals Radiative Mechanisms and Substrate Doping-Type Effects of InAs Nanowires. *Nano Lett.* **2017**, *17*, 1545−1551.

(22) Bechstedt, F.; Belabbes, A. Structure, energetics, and electronic states of III-V compound polytypes. *J. Phys.: Condens. Matter* **2013**, *25*, 273201.

(23) Anyebe, E. A.; Kesaria, M. Photoluminescence Characteristics of Zinc Blende InAs Nanowires. *Sci. Rep.* **2019**, *9*, 17665.

(24) Goosney, C. J.; Jarvis, V. M.; Britten, J. F.; LaPierre, R. R. InAsSb Pillars for Multispectral Long-Wavelength Infrared Absorption. *Infrared Phys. Technol.* **2020**, *111*, 103566.

(25) Azizur-Rahman, K. M.; LaPierre, R. R. Wavelength-Selective Absorptance in GaAs, InP and InAs Nanowire Arrays. *Nanotechnology* **2015**, *26*, 295202.

(26) Azizur-Rahman, K. M.; LaPierre, R. R. Optical Design of a Mid-Wavelength Infrared InSb Nanowire Photodetector. *Nanotechnology* **2016**, *27*, 315202.

(27) Dhindsa, N.; Chia, A.; Boulanger, J.; Khodadad, I.; LaPierre, R.; Saini, S. S. Highly Ordered Vertical GaAs Nanowire Arrays with Dry Etching and Their Optical Properties. *Nanotechnology* **2014**, *25*, 305303.